

Short-Fluorinated iCVD Coatings for Nonwetting Fabrics

Dan Soto, Asli Ugur, Taylor A. Farnham, Karen K. Gleason, and Kripa K. Varanasi*

Water repellency is often generated by taking advantage of surface textures and low surface energy coatings such as the one afforded by long perfluorinated side-chains polymers. However, new regulations are phasing out these polymers because of their related health and safety hazard concerns. This is a particular challenge for water-repellent fabrics as consumers expect safer products with stable performance and new functionalities. In this work, an approach is developed that allows for iCVD deposition of durable, conformal short fluorinated polymers stabilized with a crosslinking agent. As a result, high hydrophobicity and low liquid adhesion are achieved simultaneously while maintaining initial substrate breathability. It is explained why this polymeric coating—1H,1H-perfluorooctyl methacrylate co divinylbenzene—exhibits remarkable hydrophobic properties amidst a wide range of other possible candidates. In order to further enhance the dynamic water repellency performance, the chemical treatment is combined with physical texturing—obtained through microsandblasting, a process particularly suitable for fabrics—thus making this combined approach a suitable candidate to meet the industrial needs. This work paves the way for the development of environmentally friendly, highly repellent coatings for large volume production and the application of roll-to-roll coating techniques, and multifunctionalization of fabrics and wearable devices.

1. Introduction

Water repellency is most often generated by taking advantage of surface textures^[1,2] and low surface energy coatings such as the one afforded by polymers possessing long perfluorinated side chains.^[3–6] However, perfluorinated chains of eight carbons or more, have been shown to be persistent in the environment and bioaccumulate in living organisms.^[7] Because of the related health and safety hazard concerns, governmental agencies are phasing out and banning these polymers, requiring the search for, and use of, new chemistries with shorter perfluorinated side chains.^[8] This is a particular challenge for the water-repellent fabrics as textile coatings are commonly applied via liquid

phase processes^[9] which requires forcing the liquid into the pores, drying them without clogging and taking care of waste management. Hence, in the midst of the textile technological evolution embodied by the development of the so called “smart fabrics,” initiated chemical vapor deposition^[10] (iCVD) appears as a new promising technique; iCVD allows the deposition of the ultrathin conformal durable and breathable coatings and paves the path to new types of functionalization such as charge management capabilities.^[11]

In this work, we develop an approach that allows for iCVD deposition of conformal short fluorinated polymers stabilized with a crosslinking agent and report the successful iCVD polymerization of 1H,1H-perfluorooctyl methacrylate crosslinked with divinylbenzene. We explain why this coating having less than eight perfluorinated sidechain carbons exhibit remarkable hydrophobic properties and low adhesion amidst a wide range of other possible candidates making it a suitable candidate to replace the more persistent polymers that are being banned. In


order to further enhance the dynamic water repellency performance, we combine the chemical treatment with physical texturing done through microsandblasting, a process particularly suitable for fabrics. Finally, we show how the iCVD growth method results in durable and breathable coatings and allows to extend the range of applications to substrates as diverse as fabrics, paper, and nanotextured silicon.

2. Results and Discussions

The iCVD process is a single-step vapor-phase method used to deposit conformal polymer films with a controllable thickness^[10] and texture.^[10,12,13] In addition, the potential to graft the polymer directly to the substrate enhances coating durability.^[14,15] The side chains of these polymer films, grown through radical polymerization,^[10] play a key role in the macroscopic properties of the films. Indeed, it has been shown that the highest hydrophobicity, that is, the lowest surface energy, is chemically achieved with $-\text{CF}_3$ groups (followed by $-\text{CF}_2\text{H}$, $-\text{CF}_2$, $-\text{CH}_3$, $-\text{CH}_2$, respectively, in terms of decreasing hydrophobicity). In that perspective, side chains can be seen as fluorine carriers site (see **Figure 1a**) that lead to surface energies as low as 6 mN m^{-1} when uniformly structured.^[16] Since such low surface energies—giving rise to extremely nonwetting

Dr. D. Soto, T. A. Farnham, Prof. K. K. Varanasi
Department of Mechanical Engineering
Massachusetts Institute of Technology
Cambridge, MA 02139, USA
E-mail: varanasi@mit.edu

Dr. A. Ugur, Prof. K. K. Gleason
Department of Chemical Engineering
Massachusetts Institute of Technology
Cambridge, MA 02139, USA

 The ORCID identification number(s) for the author(s) of this article can be found under <https://doi.org/10.1002/adfm.201707355>.

DOI: 10.1002/adfm.201707355

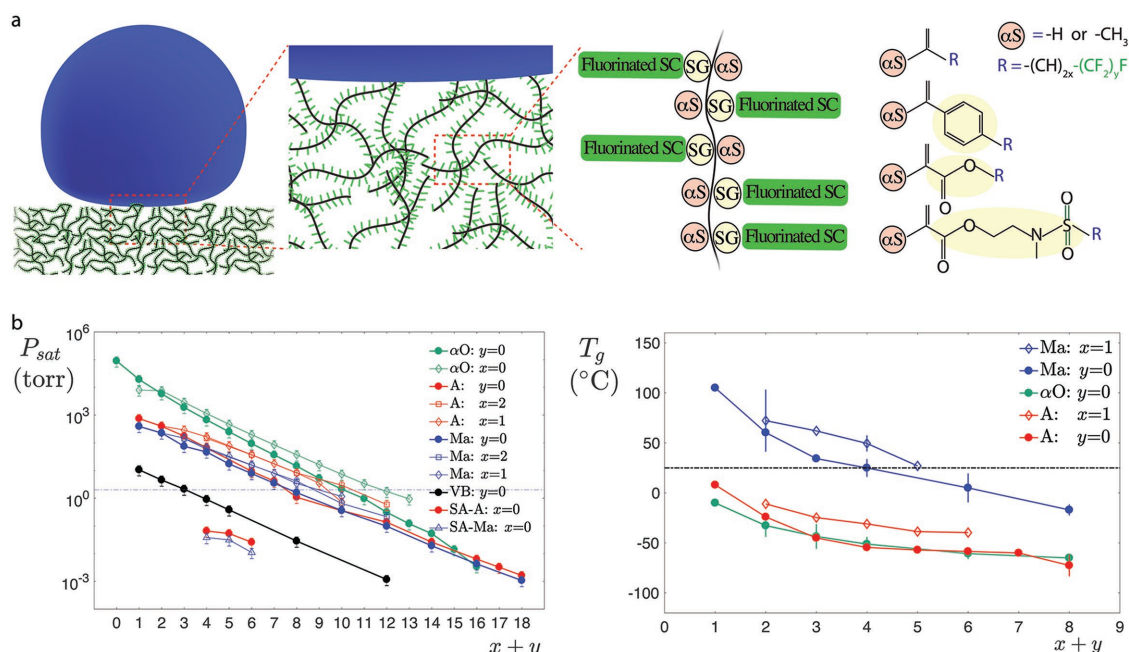


Figure 1. a) Schematic view of coating where side chains consisting of a tail can carry the fluorinated groups (fluorinated SC, solid green) and are attached to the backbone through a spacer group (SG, shaded yellow). A bulky alpha-substituent (α S, shaded red) will limit side chain mobility. Right panel: monomers suitable for free radical polymerization: olefin, vinylbenzene derivatives, (meth)-acrylate and sulfonamide (meth)-acrylate. The end of the side chain (R -) has x hydrogenated and y fluorinated carbons. b,c) Monomer vapor pressure (at 80 °C) and glass transition temperature T_g as a function of side chain length $x + y$: in green, olefins (α O); in red, acrylates (A) and sulfonamide acrylate (SA-A); in blue, methacrylates (MA) and sulfonamide methacrylate (SA-M); in black, vinyl benzene (VB). Data from literature values as described in the Supporting Information.

substrates—can only be achieved with fluorinated chemistries, traditional, and widely used silicon-based coatings do not provide suitable replacement solutions.^[17] Because side chains can reorient upon interaction with different media^[18] they can lead to increased contact angle hysteresis (CAH) and pinning. Hence, it is important to control fluorine content and minimize pendant chains reorientation ability. Up to now, long side chain fluorinated polymers have been widely used because of their ability to crystallize,^[16,19–21] yielding outstanding performances in terms of water repellency, CAH,^[22] and stability. However, another consequence of this crystallization is their difficulty to be degraded, which leads to their bioaccumulation and potential environmental and health risks and makes them unsuitable for most applications.

Recent reports explore hydrophobic short-fluorinated solutions^[16,23–25] that draw their performances from the crystallization of heavy-molecule monomers. However, due to their low volatility, they cannot be vapor deposited and face all limitations of liquid-based solutions, among which the challenge of forcing the liquid coating into the roughness or pores of the textiles—a major obstacle to coat ever smaller features. For vapor deposition approaches, the consequences of going to short-fluorinated side chain polymers (fewer than eight perfluorinated carbons) are hence drastic: the polymer will not crystallize anymore and its amorphous nature (T_g decreasing with increasing side chain length,^[26] see Figure 1c) will lead to increased side chain mobility. Considering that fluorine content needs to be kept as high as possible in order to have low surface energies and high contact angles, we need to identify the best vaporizable monomer candidate with seven fluorinated carbons (see Figure 1c

and the Supporting Information) and optimize its side chain interactions by tuning the main chain flexibility,^[27] the stiffness of the spacer group,^[25] and the geometrical hindering of substituents.^[24] The fluorinated tails can be attached to a wide range of reactive heads allowing us to select the ones which are most suitable for radical chain polymerization process:^[28] olefins, vinylbenzenes, acrylates, methacrylates, and their derivatives (see Figure 1a, forth panel). Among these options, only the monomers that are able to evaporate into the reactor chamber can be used with iCVD process (typical vapor pressure above 1 Torr). We observe in Figure 1b that although the vinylbenzene derivate (VB), the sulfonamide acrylates (SA-A), and sulfonamide methacrylates^[16,25] (SAMa) are good candidates—they have a stiff and bulky spacer group preventing chain mobility—they are too heavy to be easily vaporized. Finally, we expect that stiffer spacer group (only one-CH₂- group between the head and the fluorinated chain being the stiffest solution) as well as a bulky alpha substituent^[24] will reduce side chain mobility, suggesting 1H,1H-perfluorooctyl methacrylate (H₁F₇Ma) as the best candidate. Indeed, this lack of mobility can also be observed in Figure 1c where for a given side chain length, the highest T_g corresponds to the case of methacrylates.

In order to deposit H₁F₇Ma via iCVD, the monomer is heated at 80 °C and the vapor phase is introduced into a reactor chamber at several hundred millitorr. The gaseous initiator *tert*-butyl peroxide (TBPO) is activated via heating filaments and polymerization of a film of typical thickness 100 nm (see Table S1, Supporting Information) is enabled directly onto the surface of a flat (silicon substrate) or textured (fabric) substrate (see the detailed deposition conditions in the Supporting

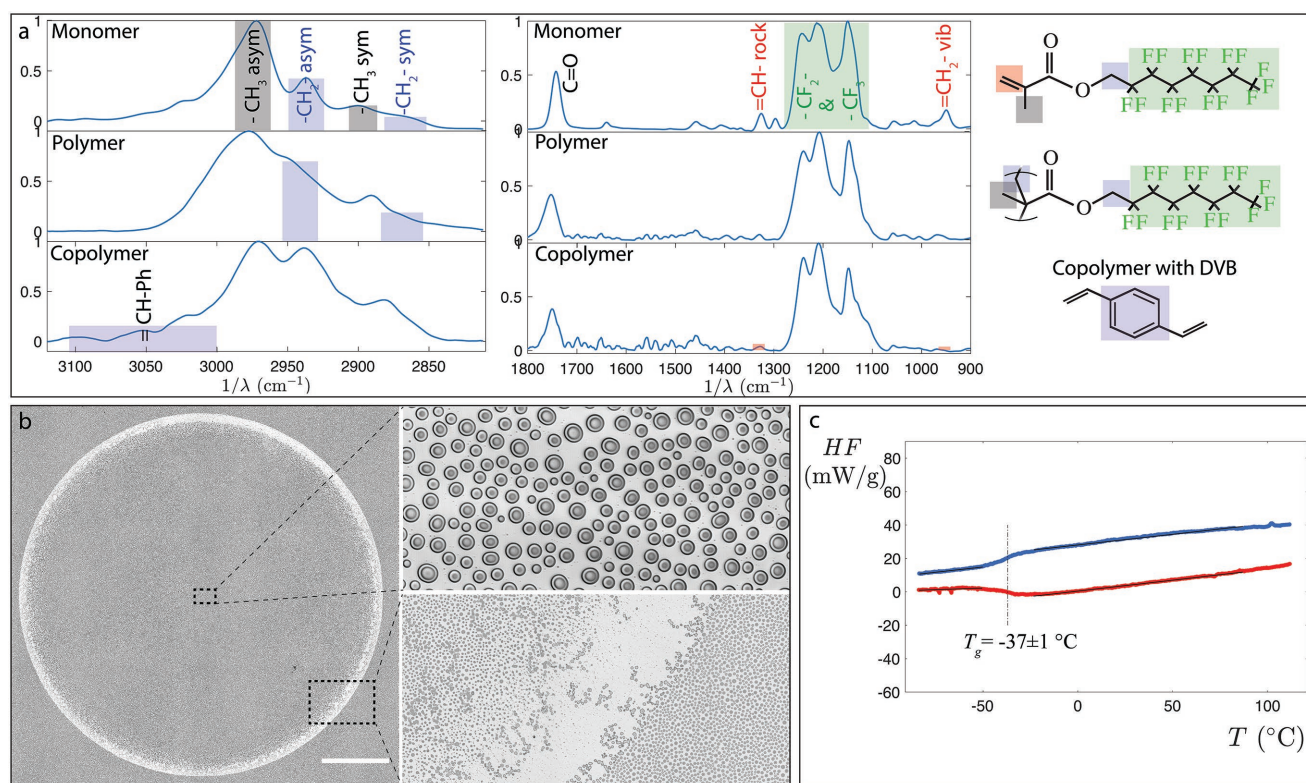


Figure 2. a) FTIR spectra of H₁F₇Ma monomer (top row), H₁F₇Ma homopolymer (middle row), and H₁F₇Ma-co-DVB copolymer (bottom row, 34% DVB content). Spectra were normalized by the -CH₃ and CF₂ & CF₃ peaks for the 2800–3100 and 900–1800 cm⁻¹ region, respectively. On the right, shaded areas correspond to functional groups highlighted in the FTIR spectra. b) Microscopic top view of a mark left on homopolymer coating on a flat silicon substrate after water droplet removal. Scale bar: 0.5 mm. Close-up views correspond to selected regions: top one shows destabilization of the coating into droplets; bottom one shows coating droplets displaced at the triple contact line after drop removal. c) Heat flux (mW g⁻¹) of H₁F₇Ma homopolymer as a function of temperature showing a glass transition temperature T_g = -37 °C.

Information). To ensure the successful polymerization of the new monomer, in **Figure 2a**, we compare its Fourier transform infrared (FTIR) spectra to the polymer. Normalizing the region 2850–3000 cm⁻¹ by the total intensity of the -CH₃ asymmetric vibration peak (gray region at 2975 cm⁻¹, expected to remain unchanged through polymerization) we can observe a relative increase of the -CH₂- asymmetric peak (blue region at 2940 cm⁻¹) for the polymer case, confirming the formation of a backbone chain. Similarly, normalizing the region 900–1400 cm⁻¹ by the intensity of the bands attributed to the -CF₂⁻, -CF₃ moieties (green region at 1146 and 1240 cm⁻¹, respectively, expected also to remain unchanged), we observe a relative decrease of the =CH- rocking and =CH₂ vibrational peaks (red regions at 1327 and 950 cm⁻¹, respectively), confirming the successful formation of the expected polymer. Although the coating deposited onto a flat silicon surface shows a very good advancing contact angle (close to the theoretical limit of 120°, see **Figure 3a**) the receding contact angle is extremely low and the water droplet exhibits considerable pinning. Indeed, when removing the drop, a visible mark is left behind (see **Figure 2b**; Movie S1, Supporting Information), an indication that the coating is not stable. Microscope examination after polymerization shows that the film has destabilized into tiny droplets^[29,30] that can be displaced by the water at the contact line,^[31] creating this unusual highly pinning behavior. To further understand this behavior,

the glass transition temperature T_g for the homopolymer is measured with differential scanning calorimetry (DSC) and found to be around -37 °C (see **Figure 2c**), in agreement with trends shown in **Figure 1c** and confirming that the coating was an elastomer allowing the film to destabilize.

To overcome this limitation we crosslink H₁F₇Ma with divinylbenzene (DVB)^[14,15] and verify the presence of the crosslinker in the copolymer by the appearance of band around 3050 cm⁻¹ (a signature of the benzene =CH bond, see **Figure 2a**) in the FTIR spectra. Indeed, when measuring the dynamic contact angle of water across copolymer coatings with different DVB content (**Figure 3a**, from 10% to 60% DVB) we observe that the film is now stabilized and retains the high hydrophobicity of the fluorinated H₁F₇Ma homopolymer as well as the low CAH of the pure DVB.

In order to find the optimal composition of the film we show in **Figure 3b** the temporal behavior of the advancing contact angle for the different DVB compositions. Below 30% DVB content, a “stick-slip” behavior can be observed due to the low crosslinking rate of DVB leading to increased CAH. Above 60% DVB, this phenomenon is suppressed but the overall hydrophobicity starts to decrease because of the lower overall fluorine content. Hence, the optimal crosslinker content is found to be between 30% and 60% DVB depending on the application needed. In what follows, we will favor having high water contact angles and we will use 30% composition as our reference.

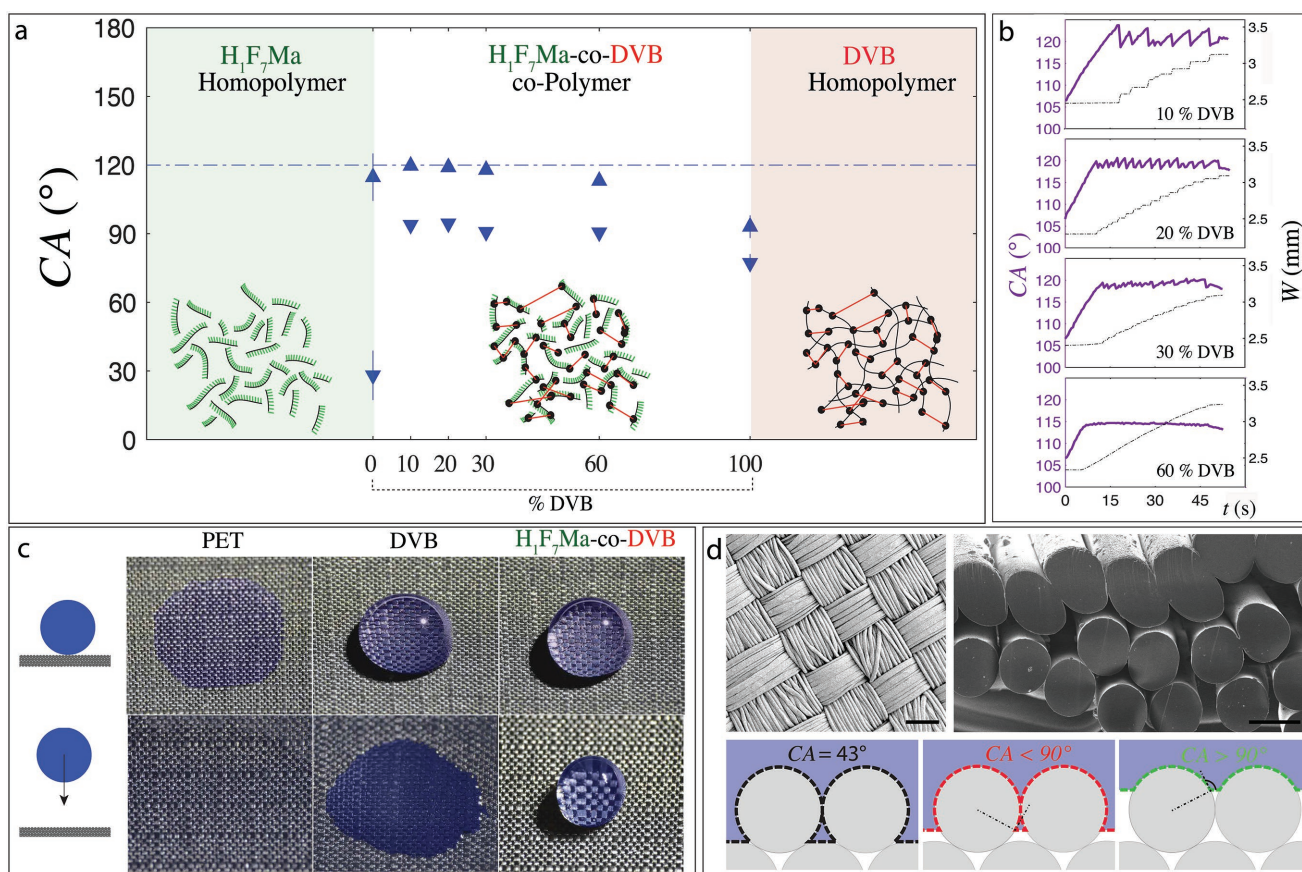


Figure 3. a) Advancing and receding contact angle (upward and downward triangle, respectively) for water measured on flat silicon substrate coated with different H₁F₇Ma and DVB contents. Sketch shows how DVB acts as a crosslinker by building bridges between backbones of different polymer chains. The dashed horizontal line marks the theoretical limit of 120°. b) Contact angle (left axis) and width W of contact area of droplet (right axis) for a droplet placed on a flat substrate coated with different DVB content and whose volume is gradually increasing from 5 to 15 μ L. c) Typical droplet outcome after being deposited (top row) or impacted (bottom row) against a polyester fabric left untreated (left), coated with DVB (middle), and coated with H₁F₇Ma-co-DVB (60% DVB, right). The wetted area has been colored with blue for increased clarity. d) SEM top view (left, scale represents 100 μ m) and cross section (right, scale represents 10 μ m) of a typical outdoor garment fabric. Impregnation model across stacked cylinders (bottom sketch): the more hydrophobic the chemistry, the more robust will be the fabric regarding water penetration.

Since iCVD coatings can be applied on a wide variety of substrates, we test and compare different polymer performance on polyethylene terephthalate polyester (PET) fabrics (20 denier warp \times 20 denier fill, taken as a reference since, together with nylon, they represent the two main outdoor fabric materials^[32]). We observe in Figure 3c and Movie S2 (Supporting Information) that without treatment, the hydrophilic nature of PET results in immediate water penetration. When coated with a DVB homopolymer (more hydrophobic than PET, see Figure S2a, Supporting Information), water will bead up if deposited gently but will still soak if impacted. Only the H₁F₇Ma-co-DVB coating will ensure extended water resistance. To understand these behaviors, we rely on the structural nature of most textiles created by weaving yarns made of the interlocked fibers (see Figure 3d) in a great variety of different patterns (see Figure 4d). By modeling their cross section as cylinders piled up in planes (typically going from three to ten layers, see sketch in Figure 3d) we assume that the condition for water penetration across the textile (different from imbibition along the fibers^[33,34]) is for the contact line at a given layer of cylinders to reach the apex of the

layer underneath it. In this framework, if the equilibrium contact angle is low (below 43°^[35]) the water will spontaneously wick the medium, as seen for nylon and PET. Between 43° and 90°, even if the substrate is hydrophilic, water will not wick spontaneously but small pressure perturbations or texture defects will allow the water to wick from one level to the next, as seen for the pure DVB coatings. Finally, in the hydrophobic case, considering that contact line has to overcome the advancing contact angle in order to infiltrate a layer of fibers, greater contact angles result in increased water repellency. Since H₁F₇Ma-co-DVB coating is very close to the theoretical limit of 120°, it emerges as an optimal solution. Besides this static performance, H₁F₇Ma-co-DVB also demonstrates suitable dynamic behavior. Indeed, if we look at a side view of a drop impacting on the different fabrics, only the H₁F₇Ma-co-DVB coating (third row in Figure 4a) allows the droplet to recoil and roll away after impact. In the other cases (untreated or 100% DVB fabrics) droplets remain attached to the fabric. As a consequence, a liquid layer can build on top of the fabric, decreasing its breathability and locally increasing the water vapor content that facilitates condensation within

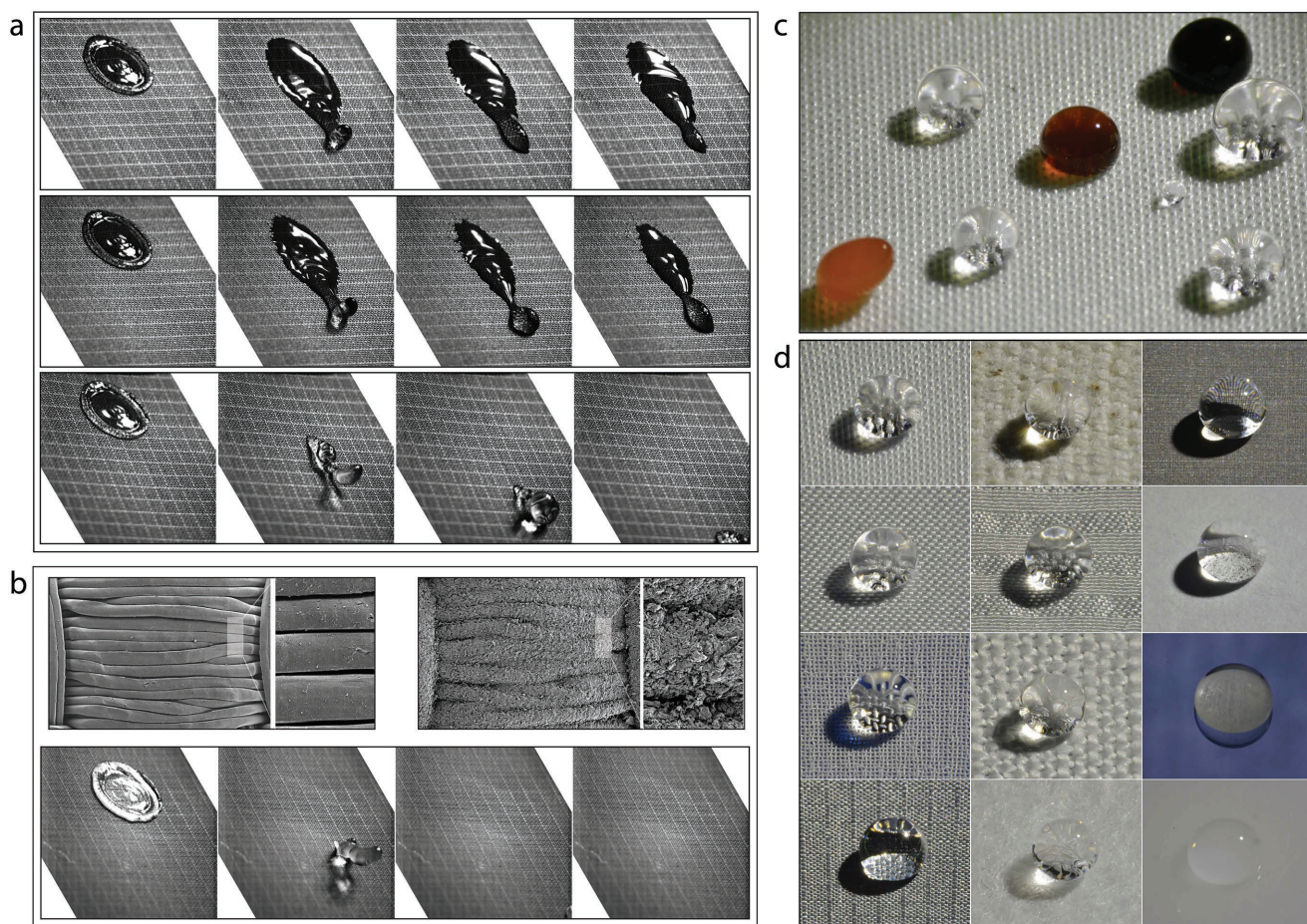


Figure 4. a) Chronophotography of a millimetric water droplet impacting on a 45° inclined substrate: bare polyester fabric (top), DVB homopolymer coated fabric (middle), and H₁F₇Ma-co-DVB coated fabric (bottom). Time between frames is 1 ms. Top and middle cases show droplet adhesion after impact and subsequent absorption by the fabric. Only H₁F₇Ma-co-DVB case shows roll off behavior and water resistance. b) Top row: SEM top view of a fabric before (left) and after (right) sand blasting with Al₂O₃ particles of grit #600. Main image and inset view correspond to a $\times 500$ and $\times 1000$ magnification factor respectively. Bottom row: Chronophotograph of drop impacting on H₁F₇Ma-co-DVB sandblasted fabric, using same conditions as in a). c) Repellency of different liquids on polyester fabric (duchesse luxury satin weave) coated with H₁F₇Ma-co-DVB: soy sauce (black drop), coffee (brown drop), ketchup sauce (orange, nonspherical drop), HCl acid (top left transparent drop), NaOH (bottom right transparent drop) and water (remaining transparent drops). d) Water deposited on different types of H₁F₇Ma-co-DVB coated fabrics. From top to bottom, first column shows different polyester weaves: duchesse satin, duchesse luxury satin, georgette and plain weave. Second column shows different organic materials: cotton, silk, linen and wool. See Movie 3 for a comparison of coated vs noncoated cotton fabric. Third column shows wide range of possible other substrates: silicon nanograss, paper, silicon wafer and nylon.

the structure. To further reduce droplet adhesion, we propose to mechanically roughen the outermost layer of the fabric by microsandblasting it and applying the coating onto the structured fabric. This process (described in the Supporting Information) was chosen because it presents several main advantages: avoiding damage of the overall mechanical properties of the fabric (as would result from chemical^[36] etching), being fast, simple, and inexpensive (as compared to plasma etching^[37]) and achieving more durable treatments (as compared to approaches based on deposition of micro and nanofeature^[38]). We observe in Figure 4b the efficient creation of a micrometric high aspect ratio texture by sandblasting a PET fabric for 10 s with 10-micron size particles. As a result, impacting droplets can now completely bounce off the surface (Figure 4b, bottom panel) instead of only being able to roll off (as observed without microtexture, Figure 4a bottom panel).

To show the versatility and performance of the iCVD technique we probe it well beyond the application of water impacting on textiles (Movie S2, Supporting Information). Indeed, from an everyday application's viewpoint, the durability of the nonwetting fabric is a critical issue. Physical damages can likely occur from abrasions, such as the one originated by the encountering between fabrics. To characterize this type of mechanical durability a laundering test consisting of 10 cold wash machine cycles was performed and no apparent wetting behavior modification was observed (see Figure 5b). In addition, abrasion tests (ISO 12947) were performed by abrading the fabric with an increasing number of strokes. Figure 5a shows how the wetting behavior of a 20 μ L water droplet remains unchanged when deposited onto an iCVD coated fabric abraded up to 10 000 times, confirming its durability (above 10 000 strokes, fiber damage and breakage became apparent).

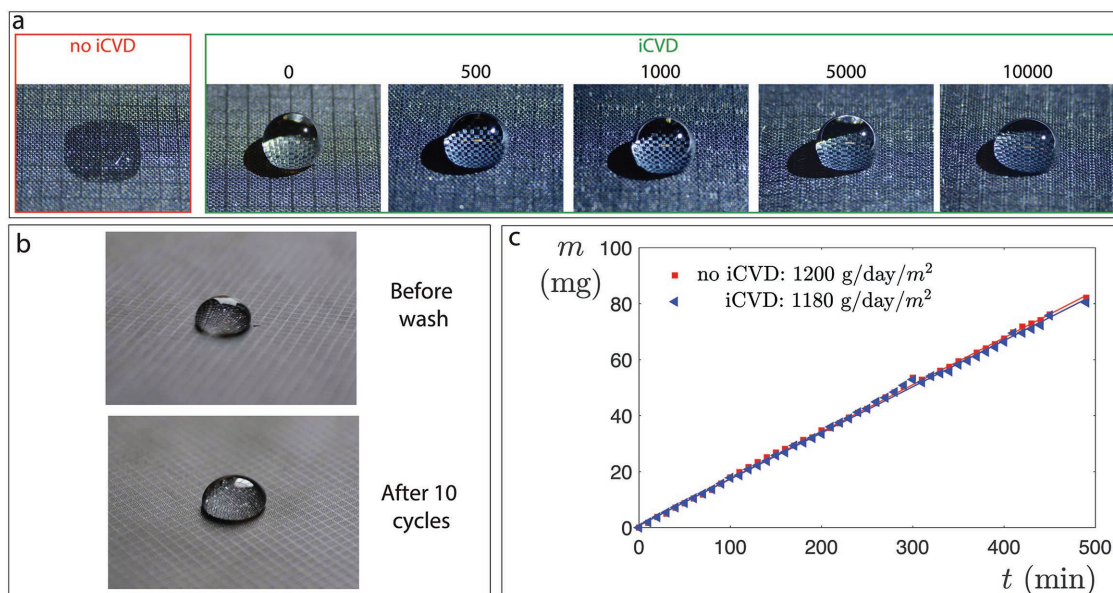


Figure 5. a) Abrasion test comparison. In red, a PET fabric (no iCVD, no abrasion) shows complete absorption of an initial water drop. In green, iCVD coated fabrics exposed to increasing number of abrading strokes: from 0 to 10000 from left to right. Pictures are taken 5 minutes after initial deposition of a 20 μL water drop. b) Water drop deposited on an iCVD coated fabric before (top) and after (bottom) 10 washing cycles. c) Evaporative mass loss as a function of time for iCVD-coated (blue) and noncoated (red) PET fabric. a, b, c) All iCVD coatings are $\text{H}_1\text{F}_7\text{Ma-co-DVB}$ (30% DVB content).

We can also observe in Figure 4c very good performance and chemical durability for a wide variety of liquids. Since we did not see any modification of the coated textiles after soaking them for 24 h in harsh acids or bases (HCl 37% and NaOH 50%), this coating can also be considered to protect surfaces from chemical exposure. In addition, since iCVD allows for ultrathin conformal coating, initial breathability of the fabric can be maintained. Indeed, Figure 5c shows how the initial breathability ($1200 \pm 20 \text{ g d}^{-1} \text{ m}^{-2}$) of a noncoated fabric remains almost unchanged after iCVD deposition ($1180 \pm 20 \text{ g d}^{-1} \text{ m}^{-2}$). The small difference (1.7% lower breathability after deposition) is in very good agreement with the 1% thickness change and emphasizes the importance of being able to deposit ultrathin coatings. Regarding low surface tension oils (see the Supporting Information) we are able to observe much slower impregnation dynamics than compared with the bare fabrics. In order to address a wider variety of substrates, we successfully coated fabrics with different weaves (duchesse, luxury duchesse, georgette, and plain), different materials (cotton, silk, linen, and wool) and even more general substrates such as flat nylon, silicon wafer, paper, and nano-textured surfaces (all showing super hydrophobic behavior, see Figure 4d).

3. Conclusion

In summary, our approach allows: 1- to tackle the EPA challenge while exploiting all advantages associated to a vapor deposition technique and 2- to extend the range of application from textiles to any type of substrates and surface coatings. Indeed, the iCVD approach has shown promise as a high-performance coating in the face of regulations banning of longer chain fluorinated polymers. The conformal, ultrathin, grafted,

and multifunctionalization aspect of iCVD leads to breathable, low material usage, durable, and EPA acceptable coatings. $\text{H}_1\text{F}_7\text{Ma-co-DVB}$ achieves an optimal balance between: surface energy, permitted carbon chain length, and polymer chain rigidity, three parameters critical in the creation of non-wetting fabrics. Additionally, a method for roughening fabrics and creating additional texture has been proposed and shown to improve the performance of the $\text{H}_1\text{F}_7\text{Ma-co-DVB}$ coating. This combined approach has yielded fabrics that repel water impacting from height, as well as oils, acids and bases even after abrasion or laundering aging. Beyond textiles, the iCVD deposition has shown applicability to a variety of substrates ranging from paper to plastics. As a consequence, this work opens the door to new solutions in the coating landscape and paves the way for development of high repellency coatings with large volume production, application of roll-to-roll coating techniques, and multifunctionalization of fabrics and wearable devices.

4. Experimental Section

iCVD Process: All iCVD depositions were conducted in a custom-built reactor previously described.^[14,15] TBPO (97%) initiator was introduced at room temperature into the chamber through a mass flow controller. It underwent activation by hot filament wires placed 2 cm above the samples. The specimen temperature was controlled via a back-cooling recirculation water system. Monomers were heated to 60 °C for DVB (80%) and 80 °C for $\text{H}_1\text{F}_7\text{Ma}$ (25G) and their flow rates were controlled using needle valves. The chamber pressure was maintained constant during the whole process using a throttle valve. Polymerization thickness was monitored in situ with laser interferometry through the transparent quartz top cover and growth was interrupted when a thickness around 100 nm was attained (typically 10 min) ensuring initial color remained unchanged after deposition. The overall composition of each compound was estimated by evaluating their partial pressure and

deducting the corresponding fractional saturation percentage. See the Supporting Information for a more detailed description.

Polymer Coating Characterization: For each deposition, a flat silicon wafer was placed into the chamber to allow postpolymerization characterization. Film thickness was confirmed through variable-angle ellipsometric spectroscopy (VASE, M-2000, J. A. Woollam), in good agreement with the in situ laser interferometric measurement. All VASE thickness measurements were performed at 60°, 70°, and 80° incidence angle using 190 wavelengths from 315 to 718 nm. A nonlinear least-squares minimization was used to fit ellipsometric data of the films to the Cauchy-Urbach model. The thickness was obtained upon convergence of the algorithm. FTIR was performed on a Nicolet Nexus 870 ESP spectrometer equipped with a mercury cadmium tellurium (MCT) detector and KBr beam splitter in normal transmission mode. For the liquid H₂F₇Ma monomer, a DTGS detector was used in combination with a liquid transmission cell (Pike, 6 µm path length). Spectra over 350–3500 cm⁻¹ with a resolution of 4 cm⁻¹ were collected and averaged over 256 scans to improve signal-to-noise ratio. All spectra were baseline-corrected. Differential scanning calorimetry (Discovery DSC, TA instruments) was used to measure the glass transition of H₂F₇Ma homopolymer by ramping up from -90 to 120 °C by 2.5 °C min⁻¹ after initial and final temperature equilibration for 5 min.

Test: Laundering test was performed in a top load washing machine and drying was allowed in between each cold wash cycle. Abrasion test ISO 12947 was performed by SDL Atlas on a M235 Martindale abrasion tester with 9 kPa pressure weight and 500, 1000, 5000 10 000 cycles on PET and cotton iCVD coated fabrics. A Lisajoux pattern and a 100% standard wool abradant were used. Breathability test (ISO 2528 A-2) was performed by measuring the evaporative mass loss through the cylindrical top open section (16 mm diameter) of a container (20 mL 27 × 57 glass vial) filled with 16 mL water covered with a PET iCVD coated fabric using a microbalance (Mettler Toledo MS). Data was recorded for 500 min in a room at 21 °C and results were compared (see the Supporting Information) to the case of an untreated fabric.

Supporting Information

Supporting Information is available from the Wiley Online Library or from the author.

Acknowledgements

The authors gratefully acknowledge funding support from Deshpande center at MIT. D.S. acknowledges funding support from Translational Fellowship Program at MIT. The authors thank A. Liu, A. Servi, and Y. Jiang for interesting discussions as well as B. Solomon, H. L. Girard, and P. Moni for help with DSC, AFM, and FTIR measurements, respectively. This work made use of the Institute for Soldier Nanotechnologies (ISN) at MIT. The authors thank M. Jansen from SDL Atlas for performing abrasion tests and T. O'Hara for providing fabrics samples.

Conflict of Interest

The authors declare no conflict of interest.

Keywords

fabrics, hydrophobic coatings, initiated chemical vapor deposition (iCVD), micro-sandblasting, short-fluorinated polymers, textiles

Received: December 19, 2017
Revised: March 19, 2018
Published online: June 29, 2018

- [1] X. Deng, L. Mammen, H.-J. Butt, D. Vollmer, *Science* **2012**, 335, 67.
- [2] M. Liu, S. Wang, L. Jiang, *Nat. Rev. Mater.* **2017**, 2, 17036.
- [3] Y. Li, S. Chen, M. Wu, J. Sun, *Adv. Mater.* **2014**, 26, 3344.
- [4] A. Tuteja, W. Choi, M. Ma, J. M. Mabry, S. A. Mazzella, G. C. Rutledge, G. H. McKinley, R. E. Cohen, *Science* **2007**, 318, 1618.
- [5] S. T. Iacono, S. M. Budy, D. W. Smith, J. M. Mabry, *J. Mater. Chem.* **2010**, 20, 2979.
- [6] A. C. Glavan, R. V. Martinez, A. B. Subramaniam, H. J. Yoon, R. M. D. Nunes, H. Lange, M. M. Thuo, G. M. Whitesides, *Adv. Funct. Mater.* **2014**, 24, 60.
- [7] OECD/UNEP Global PFC Group, Environment Health Safety, Environment Directorate, OECD, **2013**.
- [8] Environmental Protection Agency, US Environmental Protection Agency, **2009**, 12, p. 30.
- [9] G. Akovali, *Advances in Polymer Coated Textiles*, Smithers Rapra, **2012**.
- [10] A. M. Coclite, R. M. Howden, D. C. Borrelli, C. D. Petruczuk, R. Yang, J. L. Yagüe, A. Ugur, N. Chen, S. Lee, W. J. Jo, A. Liu, X. Wang, K. K. Gleason, *Adv. Mater.* **2013**, 25, 5392.
- [11] A. Ugur, F. Katmis, M. Li, L. Wu, Y. Zhu, K. K. Varanasi, K. K. Gleason, *Adv. Mater.* **2015**, 27, 4604.
- [12] L. C. Bradley, M. Gupta, *Langmuir* **2015**, 31, 7999.
- [13] H. S. Suh, D. H. Kim, P. Moni, S. Xiong, L. E. Ocola, N. J. Zaluzec, K. K. Gleason, P. F. Nealey, *Nat. Nanotechnol.* **2017**, 12, 575.
- [14] A. T. Paxson, J. L. Yagüe, K. K. Gleason, K. K. Varanasi, *Adv. Mater.* **2014**, 26, 418.
- [15] A. Liu, E. Goktekin, K. K. Gleason, *Langmuir* **2014**, 30, 14189.
- [16] Q. Zhang, Q. Wang, J. Jiang, X. Zhan, F. Chen, *Langmuir* **2015**, 31, 4752.
- [17] J. Williams, *Waterproof and Water Repellent Textiles and Clothing*, – 1st ed., (Ed: J. T. Williams), Elsevier **2017**.
- [18] J. A. Kleingartner, H. Lee, M. F. Rubner, G. H. McKinley, R. E. Cohen, *Soft Matter* **2013**, 9, 6080.
- [19] M. Beiner, H. Huth, *Nat. Mater.* **2003**, 2, 595.
- [20] K. A. O'Leary, D. R. Paul, *Polymer* **2006**, 47, 1245.
- [21] Y. Yoo, J. B. You, W. Choi, S. G. Im, *Polym. Chem.* **2013**, 4, 1664.
- [22] A. M. Coclite, Y. Shi, K. K. Gleason, *Adv. Mater.* **2012**, 24, 4534.
- [23] Q. Zhang, Q. Wang, X. Zhan, F. Chen, *Ind. Eng. Chem. Res.* **2014**, 53, 8026.
- [24] K. Honda, I. Yamamoto, M. Morita, H. Yamaguchi, H. Arita, R. Ishige, Y. Higaki, A. Takahara, *Polymer* **2014**, 55, 6303.
- [25] Q. Wang, Q. Zhang, X. Zhan, F. Chen, *J. Polym. Sci., Part A: Polym. Chem.* **2010**, 48, 2584.
- [26] F. Fleischhaker, A. P. Haehnel, A. M. Misske, M. Blanchot, S. Haremza, C. Barner-Kowollik, *Macromol. Chem. Phys.* **2014**, 215, 1192.
- [27] T. Hirabayashi, T. Kikuta, K. Kasabou, K. Yokota, *Polym. J.* **1988**, 20, 693.
- [28] G. G. Odian, *Principles of Polymerization*, Wiley-Interscience, Hoboken, NJ, USA **2004**, Ch. 3.
- [29] R. Mukherjee, A. Sharma, *Soft Matter* **2015**, 11, 8717.
- [30] *Fluid Mechanics of Surfactant and Polymer Solutions* (Eds: V. Starov, I. Ivanov), Springer, Vienna **2004**.
- [31] R. W. Style, E. R. Dufresne, *Soft Matter* **2012**, 8, 7177.
- [32] R. R. Mather, R. H. Wardman, *The Chemistry of Textile Fibers*, Royal Society of Chemistry, Cambridge **2010**.
- [33] I. Pezron, G. Bourgain, D. Quéré, *J. Colloid Interface Sci.* **1995**, 173, 319.
- [34] C. Duprat, S. Protière, A. Y. Beebe, H. A. Stone, *Nature* **2012**, 482, 510.
- [35] P. S. Raux, H. Cockenpot, M. Ramaioli, D. Quéré, C. Clanet, *Langmuir* **2013**, 29, 3636.
- [36] C.-H. Xue, X.-J. Guo, M.-M. Zhang, J.-Z. Ma, S.-T. Jia, *J. Mater. Chem. A* **2015**, 3, 21797.
- [37] B. Shin, K.-R. Lee, M.-W. Moon, H.-Y. Kim, *Soft Matter* **2012**, 8, 1817.
- [38] J. A. Kleingartner, S. Srinivasan, Q. T. Truong, M. Sieber, R. E. Cohen, G. H. McKinley, *Langmuir* **2015**.